HHS Public Access

Author manuscript

ACS Appl Mater Interfaces. Author manuscript; available in PMC 2021 September 02.

Published in final edited form as:

ACS Appl Mater Interfaces. 2020 September 02; 12(35): 38950–38961. doi:10.1021/acsami.0c10276.

Injectable, ribbon-like microconfetti biopolymer platform for vaccine applications

Kathryn M. Moore[1], **Cole J. Batty**[2], **Rebeca T. Stiepel**[2], **Christopher J. Genito**[3], **Eric M. Bachelder**[2], **Kristy M. Ainslie**[1,2,3]

[1]Joint Department of Biomedical Engineering, University of North Carolina at Chapel Hill and North Carolina State University, USA.

[2]Division of Pharmacoengineering and Molecular Pharmaceutics, Eshelman School of Pharmacy, University of North Carolina at Chapel Hill, USA.

[3]Department of Microbiology and Immunology, UNC School of Medicine, University of North Carolina, Chapel Hill, NC, USA.

Abstract

Previously, high aspect ratio ribbon-like microconfetti (MC) composed of acetalated dextran (Ace-DEX) have been shown to form a subcutaneous depot for sustained drug release. In this study, MC were explored as an injectable vaccine platform. Production of MC by electrospinning followed by high-shear homogenization allowed for precise control over MC fabrication. Three distinct sizes of MC, small (0.67 × 10.2 μm), medium (1.28 × 20.7 μm), and large (5.67 × 90.2 μm), were fabricated and loaded with the adjuvant, resiquimod. Steady release rates of resiquimod were observed from MC, indicating their ability to create an immunostimulatory depot in vivo. Resiquimod-loaded MC stimulated inflammatory cytokine production in bone marrow derived dendritic cells without incurring additional cytotoxicity in vitro. Interestingly, even medium and large MC were able to be internalized by antigen presenting cells and facilitate antigen presentation when ovalbumin was adsorbed onto their surface. After subcutaneous injection in vivo with adsorbed ovalbumin, blank MC of all sizes were found to stimulate a humoral response. Adjuvant activity of resiquimod was enhanced by loading it into MC and small and medium sized MC effectively induced a Th1-skewed immune response. Antigen co-delivered with adjuvant-loaded MC of various sizes illustrate a new potential vaccine platform.

Graphical Abstract

Corresponding Author: Kristy M. Ainslie, Professor, Division of Pharmacoengineering and Molecular Pharmaceutics, UNC Eshelman School of Pharmacy, 4211 Marsico Hall, 125 Mason Farm Road, Chapel Hill, NC 27599, United States, ainsliek@email.unc.edu.

Author Contributions

The manuscript was written through contributions of all authors. All authors have given approval to the final version of the manuscript.

Supporting Information (file type, PDF). Figures S1–S16 and Tables S1–S2 are found in the supporting information.

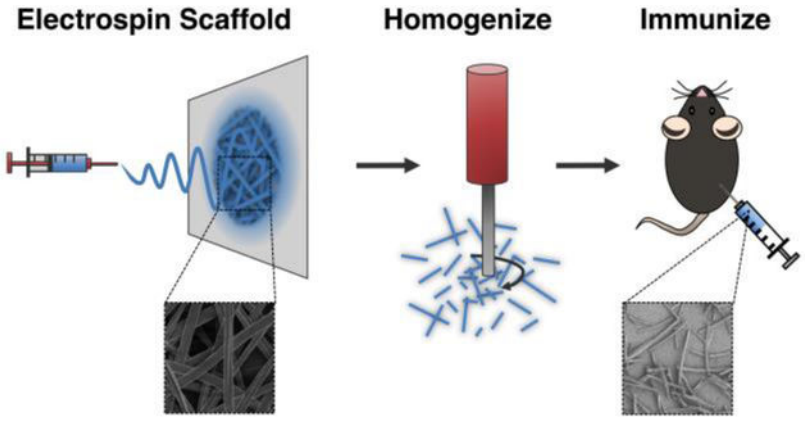

Keywords

Ace-DEX; electrospinning; resiquimod; high aspect ratio; ovalbumin

INTRODUCTION

In response to the poor immunogenicity of proteins and peptides on their own, often an adjuvant is used in a vaccine formulation to stimulate a protective immune response. Examples of FDA-approved adjuvants include the aluminum salts (alum) and emulsion-based adjuvants like MF59 (squalene oil, Span 85, Tween 80, and citrate buffer) and AS03 (squalene and DL-α-tocopherol, a more bioavailable form of vitamin E)[1–3]. Many of these adjuvants serve as depots that create a reservoir at the site of injection for extended stimulation of antigen presenting cells (APCs). This approach has led to an enhanced adaptive immune response compared to saline controls[2–4].

In addition to depot-like approaches, the use of pathogen-associated molecular patterns (PAMPs) as adjuvants has also been applied to FDA-approved vaccines. PAMPs bind to pattern recognition receptors, such as toll-like receptors (TLRs), to trigger potent innate signaling. Examples of PAMP-containing adjuvants are AS04, CpG and AS01B, which are formulated into a wide variety of vaccines. TLR agonists (e.g. CpG and monophosphoryl lipid A (MPL)) are viewed as promising vaccine adjuvants because they can enhance type 1 helper (Th1) cellular immunity against intracellular pathogens, whereas most depot-forming adjuvants primarily skew towards a type 2 helper (Th2) phenotype[5–6]. Additional TLR agonists have been investigated preclinically, such as resiquimod, the TLR 7/8 agonist imidazoquinoline that mimics single-stranded viral RNA[7]. Resiquimod (also known as R-848) was developed by 3M (St. Paul, MN) and has demonstrated 10–100x more potent adjuvant activity compared to its analog, Imiquimod (Aldera®), an FDA-approved topical adjuvant[8]. Resiquimod has illustrated protection and potent Th1 responses pre-clinically as a vaccine adjuvant for a variety of vaccines including anthrax[9–10], melioidosis[11], melanoma[12], and HIV[13].

Combining depot forming adjuvants with a TLR agonist has been a strategy to create a more balanced Th1/Th2 response. For example, AS04, the adjuvant used in the human

papillomavirus vaccine Cervarix®, is a mixture of alum and MPL. Combining MPL with alum was found to extend the duration of cytokine production afforded by MPL and correlated with higher numbers of activated APCs in the lymph nodes[14]. Cervarix® stimulated higher serum antibody titers and memory B cells compared to Gardasil®, another HPV vaccine that uses very similar antigens, but contains only alum as the adjuvant[15].

Biomaterial scaffolds have recently emerged as another method to enhance vaccine efficacy by serving as an immunostimulatory depot. In a seminal study, Ali et al. found that poly lactic-co-glycolic acid (PLGA) foams loaded with tumor lysate, a dendric cell maturation agent (granulocyte-macrophage colony-stimulating factor, GM-CSF) and TLR agonist CpG provided a persistent, antigen-rich environment with immunostimulatory signals that generated an anti-tumor immune response through recruitment and stimulation of APCs and T cells[16]. A number of other scaffolds have since been explored as vaccine adjuvant depot platforms, such as hydrogels composed of dextran[17], alginate[18], poly (L-valine)[19], poly(ethylene glycol)-PLGA[20], chitosan[21–22] and poly(2-hydroxyethyl methacrylate) with poly(dimethylsiloxane)[23]. Similarly, mesoporous silica rods (MSRs) have also been shown to self-assemble into a 3D immune depot capable of stimulating robust immune responses[24–26].

In many of these scaffold vaccines, antigen and adjuvant are loaded within the scaffold to be released in a soluble form. Release of these vaccine elements from a large scaffold provides less control over antigen delivery to APCs, limiting potential antigen presentation. Nano- and microparticles have frequently been used to efficiently deliver antigen and adjuvant in biomaterial vaccines because they can be internalized by APCs[27–28]. As such, several scaffolds have loaded nano- or microparticles within the scaffold to target APCs; however, this adds substantial complexity to the system. Development of a simplified platform that allows for more effective and controlled vaccine element delivery, while also maintaining long-term persistence of the vaccine depot, could be a beneficial next step in scaffold vaccine development.

In this study, we characterize a novel injectable vaccine platform composed of the biodegradable polymer acetalated dextran (Ace-DEX) formulated as high aspect ratio, ribbon-like particles termed microconfetti (MC). We hypothesize that MC create a 3D depot in the subcutaneous space upon injection and offer an advantage over scaffold-based vaccines that require surgical implantation. MC were first developed for long-acting delivery of antiretroviral drugs to treat HIV, to deliver sustained drug release to reduce frequency of drug administration[29]. MC were fabricated by mechanically fragmenting electrospun scaffolds, and were found to retain the ability of electrospun scaffolds to provide sustained drug release[29–31]. In this way, MC combine the favorable characteristics of both microparticle and scaffold-based vaccines. Ace-DEX was chosen as the polymer platform based on its compatibility with a wide range of electrospinning solvents, acid sensitivity, pH neutral byproducts, and tunable degradation[32]. Notably, the tunable degradation of Ace-DEX has been shown to enhance antigen presentation by APCs and drug release profiles from microparticles and scaffolds, making it a desirable foundation for immunomodulatory platforms[31, 33–34]. Furthermore, among the other common polymers (PLGA and polycaprolactone) evaluated for MC, Ace-DEX was the only polymer that did not melt

during the process of fragmenting the fibers due to the polymer's high glass transition temperature[29].

Herein, MC were fabricated with and without resiquimod in three unique sizes by tuning electrospinning parameters. APC internalization of formulated MC, as well as the resulting cytokine release and antigen presentation, were evaluated in vitro. In vivo, the effect of formulated MC on humoral immune response was assessed against a model antigen.

RESULTS AND DISCUSSION

Fabrication and characterization of microconfetti

In this study, MC were fabricated by homogenizing electrospun scaffolds in water, then subsequently lyophilizing to achieve a dry powder (Figure 1A). Changes in electrospun scaffold fiber diameter were found to be the main parameter for tuning MC dimensions (Figure 1A–D). The electrospun scaffold fiber diameter remained unchanged by homogenization. Interestingly, on average, scaffold fiber width indirectly affected the length of the MC after homogenization, where length was defined as the two ends fragmented by homogenization. Interestingly, on average, the MC length depended greatly on the electrospun scaffold fiber diameter, where wider fiber diameters resulted in longer MC fragments. By increasing both electrospinning polymer concentration and flow rate, longer MC fragments were achieved, while reducing those parameters lent to thinner fiber diameters and shorter MC (Figure 1B–D). Variations in homogenization speed and length of time were not influential in changing the resulting MC length (data not shown). A panel of scaffolds were electrospun by tuning polymer concentration and flow rate (Figure S1) to fabricate three MC populations of different sizes. The resulting three MC populations with distinct widths (Figure 1C, F) and lengths (Figure 1D, F) were defined as small (W: 0.67 μm ± 0.16, L: 10.2 μm ± 4.45), medium (W: 1.28 μm ± 0.28, L: 20.7 μm ± 8.61), and large (W: 5.67 μm ± 1.01, L: 90.2 μm ± 46.3). Average aspect ratios (length:width) were maintained across all three populations, around 15–16 (Figure 1F). Despite the magnitude of their length, MC of all three sizes were able to be injected through a 26 G needle, negating the need for surgical implantation, which is an advantage for immunization (Figure 1E). Lastly, the potent toll-like receptor (TLR) 7/8 agonist, resiquimod (R-848), was loaded into MC (Figure 1F, Table S1) to serve as an adjuvant.

In vitro bioactivity of microconfetti

Release of resiquimod from small, medium, and large MC was assessed in vitro over 42 days (Figure 2A). Initial burst release of resiquimod in the first 24 hours was the highest for small MC (49.3% ± 0.87), followed by medium MC (21.1% ± 2.30), and then large MC (8.6% ± 0.06) (Table S2). A size dependent trend was also seen where decreasing MC size resulted in more rapid steady state release of resiquimod. It took 1.2 days for 50% resiquimod release from small MC, followed by 19.2 days by medium MC, and large MC released at the slowest rate, where less than 50% resiquimod was released by day 42 (Figure 2A, Table S2). This is likely due to changes in degradation or the surface area to volume ratio impacting drug diffusion. As MC size decreases the surface area to volume ratio increases leading to faster drug release. MC appeared to release resiquimod more slowly

compared to previously fabricated spherical Ace-DEX microparticles (MPs), likely due to a combination of their size and shape. Duong et al. fabricated electrosprayed Ace-DEX MPs slightly smaller than small MC (1 – 5 μm) and at half the weight loading (0.54%) of resiquimod had released all resiquimod at pH 7.4 within two days[35]. The slower and controlled release of adjuvant distinguishes MC from spherical particle systems and may provide more long-term immune stimulation in vivo as a vaccine depot.

Treatment of bone marrow derived dendritic cells (BMDCs) with MC resulted in dose dependent cytotoxicity in vitro after 24 hours (Figure 2B–C, Figure S3A–B). A size dependent trend in cytotoxicity was observed, where decreasing MC size resulted in increased cytotoxicity in BMDCs for both blank (Figure 2B) and resiquimod-loaded MC (Figure 2C). Because MC were unable to be fabricated with other commonly used biodegradable polymers such as PLGA, head to head comparisons with MC could not be performed. Although, previously, PLGA MPs were found to induce comparable cytotoxicity to Ace-DEX MPs[36]. Small and medium blank MC induced a level of cytotoxicity comparable to spherical Ace-DEX MPs (Figure 2B, Figure S3A). Taken together, these results suggested that neither the polymer, nor the ribbon-like shape of MC dramatically altered their cytotoxicity compared to spherical particle shapes.

Around 1% w/w loading of resiquimod did not enhance cytotoxicity of MC (Figure 2C) compared to blank MC (Figure 2B), which was expected considering that comparable doses of soluble resiquimod resulted in negligible cytotoxicity (Figure S3B). However, loading resiquimod in MC did stimulate inflammatory cytokine secretion. Notably, resiquimod loading increased TNF-α secretion 1–2 logs over MC blank counterparts (Figure 2D–F). Resiquimod-loaded MC stimulated levels of TNF-α secretion within the same range as soluble resiquimod (Figure S3D), with the exception of lower doses of large MC. Similar trends in small and medium MC TNF-α secretion may be related to internalization of MC, which was later evaluated. These similarly high level of secretion suggest that the small and medium MC were saturating with cells with enough resiquimod to achieve this level of TNF-α production. Although there is cytotoxicity at higher concentrations of MC, even at lower concentrations there was considerable secretion of TNF-α, suggesting that the MC are inherently bioactive and TNF-α secretion is not dependent on MC mediated cell killing. Secretion of the inflammatory cytokines IL-1β and IL-6 also increased significantly with resiquimod loading in MC (Figure S4).

Evaluation of microconfetti internalization by antigen presenting cells

As APCs, dendritic cells (DCs) are a critical target for vaccines because they are responsible for processing protein antigens and presenting them to T cells to mount an immune response[37]. For this reason, BMDCs were assessed for their ability to internalize MC by confocal microscopy (Figure S5). Small, medium, and large BODIPY-loaded MC were fabricated for fluorescent visualization. All three sizes of MC were found to be internalized by BMDCs, defined as complete surrounding of LysoTracker dye, observed in a z-stack (Figure 3A, Figure S6–7). This is most surprising for the medium (L: 20.7 μm ± 8.61) and large (L: 90.2 μm ± 46.3) MC, which in many cases were found to be as long or longer than the BMDCs (approximately 20 μm). Furthermore, adsorption of LysoTracker dye to the

surface of some internalized MC suggests that the MC eventually become exposed to the acidic microenvironment of the endosome/lysosome. This phenomenon was observed for all MC sizes and was most dramatic in the small MC group, as seen in Figure 3A. Unlike the other sizes where most of the LysoTracker red dye localized in small, circular vesicles, in cells treated with small MC, the LysoTracker red dye depicted rod-like shapes that were the same size and geometry as the small MC themselves. While all three sizes of MC were found to be internalized by BMDCs (Figure 3A), unsurprisingly, smaller MC have a higher incidence of uptake compared to medium and large MC (Figure 3C). Additionally, there was a trend of fewer MC internalized as MC size increased. The average number of medium and large MC that were internalized per cell were 2.69 ± 0.22 and 0.18 ± 0.05, respectively (Figure S8A). Too many small MC were internalized to be quantified accurately. Among the cells that had at least one MC internalized, only 1.00 ± 0.00 large MC was internalized per cell and 3.47 ± 0.51 medium MC were internalized (Figure S8B). Similar trends were observed with other commonly used cells lines for MC internalization studies, RAW 264.7 macrophages (Figure S9–10), DC2.4 DCs (Figure S11).

While several studies have investigated the effect of size on internalization of high aspect ratio particles, the particle sizes typically ranged between 0.3 and 10 μm in length, which were either smaller than small MC or the same size[38–40]. One exception is the stretched worm-like polystyrene particles investigated by Champion et al., which were around 20 – 25 μm in length, similar in average length to the medium size MC[41]. These particles were internalized by rat macrophages (NR8383) at extremely low frequency compared to spherical particles and on average less than 0.5 worm-like particles were internalized per cell at 22 hours compared to 1.5 – 2 for spherical particles. Their hypothesis for this phenomenon is that the ability of a macrophage to form an actin ring around the particle at the point of contact to drive the membrane down the particle is necessary for the particle to be internalized[41–42]. Formation of this structure requires there to be less than 45° between the membrane normal and the point of contact on the particle due to the high metabolic expenditure required. As such, they observed that their oblong shaped particles with high aspect ratios are only internalized when the macrophage comes in contact with either end of the particle, and not when approached along the middle[42].

Here, we observed that our high aspect ratio MC at a comparable length (medium MC) were internalized at a much higher frequency compared to the polystyrene worm-like particles. It is notable that Champion et al. treated cells with 30 particles per cell seeded, whereas we treated cells with a fixed mass of 12.5 μg MC which resulted in varied number of MC per cell seeded depending on the size. However, despite these differences in experimental design, BMDCs (Figure 3A) and RAW 264.7 (Figure 3B) macrophages can be seen wrapping around the middle of medium and large MC, the orientation that did not result in complete internalization for worm-like polystyrene particles in NR8383 cells. Furthermore, in many images acquired, the LysoTracker dye appears to be spreading down the MC towards the ends to further engulf the MC. This was particularly apparent in the 3D renderings of cells treated with large MC (Figure S7, Figure S10). The cells appeared to be viable, suggesting that the MC was not puncturing the cells, but rather the cell membrane was spreading along the surface of the MC. Perhaps the ribbon-like geometry of the MC, with a very short height relative to the width, creating an acute angle that may allow cell

spreading and formation of an actin ring around the particles more easily than other cylindrical or rod shaped particles with wider and more rounded edges, such as the worms from Champion et al.[41]. It is also possible that differences in particle material properties resulting in different stiffness[43] or surface chemistry[44–45] are responsible for the enhanced internalization of MC.

Nevertheless, the ability of APCs to internalize MC indicates that they can readily function as delivery vehicles for antigen and adjuvant in a vaccine.

Adsorption of ovalbumin to the surface of microconfetti

The adsorption of the model protein antigen, ovalbumin (OVA), to the surface of MC was investigated by flow cytometry (Figure 4, Figure S12–13). Within 20 minutes of co-incubation in PBS at room temperature, OVA was found to adsorb to almost all medium and large MC (99.3% ± 0.08, 96.8% ± 0.91, respectively), and was detectable for around half of the small MC (52.4% ± 2.8) (Figure 4A). The extent of OVA adsorption was quantified by OVA median fluorescence intensity (MFI) comparing MC incubated with and without OVA (Figure 4B). There was a significant increase in OVA MFI for each MC size when incubated with OVA, as well as significantly higher OVA MFI for both medium and large MC compared to small MC when incubated with OVA (Figure 4B). MC size was distinguished by forward scatter (FSC, Figure S13A), and was used to evaluate the relationship between OVA adsorption (OVA MFI) and size (Figure S13B). There was a significant correlation between OVA adsorption and MC size, determined by Pearson's correlation ($r = 0.09$, p-value = 0.001). The OVA likely adsorbs to the MC through hydrophobic interactions. Hydrophobic regions within the OVA molecules may be interacting with the hydrophobic surface of the Ace-DEX MC. Indeed, others have shown that OVA readily adsorbs onto the hydrophobic polymer PLGA[46]. The ability of protein antigen to readily adsorb to the surface of MC circumvents the need for more complicated formulation methods such as encapsulation or covalent conjugation which can subject the antigen to denaturing conditions.

Furthermore, combining OVA with blank MC resulted in the functional outcome of enhanced OVA peptide presentation on major histocompatibility complex (MHC) I (Figure 4C) and II (Figure 4D) by DCs in vitro. In the presence of co-stimulatory signals and inflammatory cytokines, presentation of antigen on MHC I and II molecules by APCs (notably, DCs) to antigen specific CD8+ and CD4+ T cells, respectively, results in their activation[47–48]. Presentation assays were performed using B3Z (CD8+) and KZO (CD4+) T cell hybridoma lines and compared to soluble OVA alone. While maintaining a consistent 10 μg dose of OVA, MC treatment concentration was varied to measure the role of MC in presentation. OVA peptide cross-presentation on MHC I was enhanced by all sizes of MC compared to soluble OVA (Figure 4C). Cross-presentation is a crucial process for eliciting effective immune responses against tumors and intracellular pathogens through the generation of CD8+ T cells[49]. Interestingly, the medium MC was the optimal size for cross-presentation on MHC I (Figure 4C). This could be due to the higher level of OVA adsorption observed on medium sized MC compared to the small MC, combined with its relatively high incidence of internalization observed in Figure 4B. In contrast, while large MC had the

highest OVA adsorption, fewer cells overall internalized the large MC (Figure 3C), which may explain the low overall MHC presentation. However, the higher antigen presentation of OVA peptide observed in cells treated by large MC compared to soluble OVA may be a result of OVA delivery via the large MC, suggesting that APCs with internalized large MC are remaining capable of antigen processing. OVA adsorption to MSRs has been previously shown to enhance MHC I presentation by DCs[26].

Previous studies have shown that biodegradable particles encapsulating OVA enhance MHC I presentation compared to soluble OVA[50–51]. Rapidly degrading Ace-DEX MPs with encapsulated have been shown to exhibit superior cross-presentation of OVA peptide compared to MPs composed of slower degrading Ace-DEX, PLGA, and iron oxide, suggesting that the process of degradation enhances the escape of antigen into the cytosol for MHC I presentation[33]. In this study, at all concentrations of MC, MHC I cross-presentation was higher for the medium MC compared to spherical electrosprayed MPs when OVA was adsorbed to the surface. This highlights the ability of MC to efficiently deliver surface adsorbed antigen to APCs, compared to a conventional spherical particle control. The mechanism of cross presentation could be that OVA is getting to the cytosol, which is increasing MHC I presentation. In Figure S5, we potentially see lysosomal disruption in BMDCs. This is supported in our previous publication where we shown that Ac-DEX MPs can induce lysosomal escape[52].

For MHC II presentation, a size dependent trend emerged, where decreasing size was more effective at enhancing presentation, with small MC outperforming other MC sizes and MPs (Figure 4D). CD4+ T cells activated by MHC II presentation are responsible for promoting a more robust humoral response[49, 53]. It is notable that loading resiquimod into medium MC did not enhance the benefit of MHC I or II presentation provided by blank MC (Figure S14). Taken together, these results demonstrate the simplicity of the MC platform and its efficacy in facilitating both MHC I and II presentation of OVA peptide. Encouraged by these results, we evaluated the potential for MC to elicit a robust immune response in vivo.

Humoral immune response to MC ovalbumin vaccine in vivo

The ability of MC to form a stable depot in vivo was verified by injecting medium sized indocyanine green (ICG)-loaded MC subcutaneously and measuring ICG fluorescence by an in vivo imaging system (IVIS). The MC depot remained at the injection site for a least 9 days (Figure S15). Next, the dose of resiquimod delivered either by MC or in soluble form was evaluated in an OVA vaccine model in vivo (Figure 5). Mice were immunized on Days 0 and 21, and serum was collected on Day 28 to measure anti-OVA antibody titers. Five batches of medium sized MC with increasing weight loadings of resiquimod were used in order to deliver increasing doses of resiquimod (0, 0.02, 0.1, 1, and 10 μg/mouse) while maintaining the same mass of MC delivered to each mouse (Table S1, Figure S16). Interestingly, all MC groups resulted in significantly higher total anti-OVA IgG titers compared to OVA only, and there was no effect from resiquimod dose delivered by MC (Figure 5A). This is similar to our findings in vitro where blank MC were efficient at MHC I cross-presentation and unaffected by resiquimod loading, suggesting that the MC themselves are immunologically active without adjuvant loading. All resiquimod-loaded MC

demonstrated enhanced total IgG titers compared to soluble resiquimod combined with OVA (Figure 5A). Furthermore, all MC groups afforded total IgG titers comparable to alum combined with OVA, a widely used adjuvant in many FDA-approved vaccines (Figure 5A)[2, 54]. Similar trends were observed with the IgG1 antibody subtype (Figure 5B).

TLR agonists have previously been combined in vaccine formulations to promote skewing of a Th1 phenotype, which contributes to the generation of a cellular immune response driven by effector CD8+ T cells[5, 7, 14]. Resiquimod is a TLR 7/8 agonist and has previously been shown to promote Th1 skewing in pre-clinical vaccine formulations[55–56]. However, in this study no dose of soluble resiquimod tested was able to generate this response over PBS or OVA. Only upon delivery via MC was the highest dose of resiquimod (10 μg) found to be effective in producing IgG2c anti-OVA antibody subtype, which is indicative of a Th1 skewed immune response (Figure 5C). This indicates that MC formulation may increase the potential for resiquimod to promote a Th1-skewed response. Alum did not result in detectable IgG2c antibodies, which was expected as it has historically promoted a Th2 immune response[54]. These results illustrate the flexibility of MC to generate a more balanced immune response depending on the adjuvant loaded.

Next all three sizes of MC with and without resiquimod loading were evaluated in the OVA vaccine model (Figure 6). All blank MC sizes were found to produce similar levels of total IgG (Figure 6A) and no detectable IgG2c (Figure 6B). These results suggest that the differences between size observed with blank MC internalization and MHC presentation in vitro were not influential enough to produce difference in the humoral response in vivo. Comparable to the results from the previous OVA vaccine study assessing resiquimod dose (Figure 5), medium blank MC, along with small blank MC, produced the same level of total anti-OVA IgG as alum, suggesting that no additional adjuvant is necessary for MC to mount a strong humoral response within the small – medium size range. Although the amount of IgG produced by large blank MC was not significantly lower than small and medium MC, it was significantly lower than alum. Furthermore, large blank MC resulted in titers more closely aligned with soluble OVA. Because the same mass of MC was delivered across the MC groups, substantially fewer large MC particles were administered compared to small and medium MC, reducing the incidence of MC interaction with APCs. This, combined with the lower overall frequency of large MC internalization in vitro, could explain the limited impact of large MC on the humoral response. Similar to other depot forming adjuvants, blank MC were found to adsorb OVA and enhance MHC presentation[2]. Furthermore, in a previous study, Kumar et al. investigated spherical and rod-shaped polystyrene particles in an OVA vaccine model and found that their un-adjuvanted rod-shaped particles also promoted a primarily Th2 response, as indicated by high anti-OVA IgG1 titers and the absence of the Th1 skewed subtype, IgG2a (for BALB/c mice)[39].

With resiquimod loaded MC, size was a more influential parameter in the humoral immune response. Small and medium resiquimod-loaded MC vaccines resulted in higher total IgG anti-OVA antibody titers compared to large MC (Figure 6A). Furthermore, small and medium blank MC produced comparable levels of total IgG titers as their resiquimod-loaded size counterparts. Interestingly, large MC was the only size to differ in titer level produced based on resiquimod-loading, yet here, resiquimod-loaded large MC resulted in lower total

IgG titers compared to blank (Figure 6A). Small and medium resiquimod-loaded MC both stimulated IgG2c production. However, small exhibited the strongest Th1 skewed response among MC sizes and was the only group that significantly increased IgG2c titers over OVA alone (Figure 6B). Considering the enhanced MHC I cross-presentation of MC observed in vitro and the production of IgG2c antibodies in vivo, small and medium resiquimod-loaded MC could likely be used to induce a cellular immune response. In contrast, large resiquimod-loaded MC did not elicit any IgG2c antibody titers (Figure 6B). It is unclear if this is due to size or its slow release profile observed in vitro (Figure 2A).

MSRs are high aspect ratio particles that have previously been investigated as biomaterials-based vaccines[24–26]. MSRs with adsorbed GM-CSF and the TLR 9 agonist, CpG, were found to enhance Th1 and Th2 skewed antibody production and immune protection in a prophylactic cancer model[24]. Interestingly, longer MSRs (88 μm) that were similar in length to large MC, were found to recruit a greater number of DCs to the injection site, which correlated with higher antigen presentation and germinal center B cells in draining LNs, compared to 37 μm long MSRs, which fall within the range of medium size MC[24]. The authors attributed this to increased pore size within the 3D depot created by the longer MSRs; APC internalization was not investigated due to their length. In this study, large MC loaded with resiquimod resulted in lower total IgG antibody production compared to medium and small MC. Other studies have also found that biomaterial scaffold pore size influences DC recruitment and infiltration[23, 57]. One possible explanation for the superior humoral response by small and medium MC is that the higher incidence of small and medium MC internalization observed in vitro could be more influential compared to the impact of depot architecture. Overall, these results demonstrate that MC are a promising vaccine platform that can be tuned by size and adjuvant loading to elicit a desired immune response.

CONCLUSIONS

Herein, the injectable, depot-forming MC platform was investigated for the first time for the application of a vaccine. Both MC size and adjuvant (resiquimod) loading were explored as tunable parameters and were found to generate different immune responses. Three distinct populations of MC were fabricated with lengths ranging from 10 – 90 μm and widths ranging from 0.7 – 5.5 μm. All sizes of MC were found to be internalized by DCs and macrophages. OVA readily adsorbed to the particle surface and MC facilitated improved MHC I and II presentation by DCs. The adjuvant activity of resiquimod was enhanced when loaded into MC in an OVA vaccine model in vivo. All three MC sizes elicited a humoral immune response and stimulated production of anti-OVA IgG antibodies after subcutaneous immunization. When delivering 10 μg of resiquimod, small and medium resiquimod-loaded MC resulted in Th1 skewing as indicated by increased IgG2c titers, whereas large MC exhibited a primarily Th2 immune response. These results illustrate the potential for the MC vaccine platform to tailor a range of immune responses by changing size and loading of resiquimod.

MATERIALS AND METHODS

All materials were acquired from Sigma (St. Louis, MO) unless otherwise indicated.

Synthesis of acetalated dextran (Ace-DEX)

Ace-DEX was synthesized as previously described[51]. Briefly, lyophilized dextran (MW 450–650 kDa) and pyridinium p-toluenesulfonate (acid catalyst) were dissolved in anhydrous dimethyl sulfoxide (DMSO). The dextran was reacted with 2-ethoxypropene (Matrix Scientific, Columbia, SC) in DMSO for 2 hours under anhydrous conditions, after which the reaction was quenched with the addition of triethylamine (TEA). The mixture was precipitated dropwise into basic water (0.04% v/v TEA in water) and lyophilized overnight. Next, the polymer was dissolved in ethanol, centrifuged to remove impurities, re-precipitated into basic water, and then lyophilized. The final product, Ace-DEX, was stored at −20˚C until further use.

Microconfetti fabrication

Electrospun Ace-DEX scaffolds were fabricated as previously described[29]. Briefly, Ace-DEX polymer was dissolved in a tri-solvent of hexafluoroisopropanol, 1-butanol, and TEA at a ratio of 59%, 40%, 1% v/v, respectively. Electrospun scaffolds were fabricated with a range of fiber diameters by changing polymer concentration and flow rates to create scaffolds with three unique widths (Figure S1). Polymer concentrations of 225, 300, and 400 mg/mL were chosen for small, medium, and large MC, respectively. The polymer solution was pumped out of a glass syringe fitted with a 21-gauge blunt needle 16 cm away from a metal collection plate with a voltage bias of 15 kV. Three different flow rates were used depending on fiber diameter size: 0.25, 1, and 4 mL/hour for small, medium, and large, respectively. Resiquimod-loaded and BODIPY-loaded scaffolds were fabricated in the same manner, with the addition of 1 w/w% resiquimod (Enzo Life Sciences, Inc., Farmingdale, NY) or 0.25 w/w% BODIPY 493–503 (Thermo Fisher Scientific) to the polymer solution, respectively. Electrospun scaffolds were collected from the collection plate and weighed.

To make the MC, scaffolds were submerged in basic water at 20 mg/mL and homogenized for 30 seconds at 21,000 RPM using an IKA® T25 digital ULTRA-TURRAX homogenizer. The resulting MC was lyophilized and stored at −20˚C until further use. Resiquimod loading was determined by dissolving samples in dimethylsulfoxide (DMSO) and reading fluorescence in a plate reader (excitation: 260 nm, emission: 360 nm) alongside a standard curve. The following equations were used to determine resiquimod loading and encapsulation efficiency: $Resiquimod\ Loading = \frac{Mass\ of\ Resiquimod}{Mass\ of\ Microconfetti} x100\%.$ $Resiquimod\ Encapsulation\ Efficiency = \frac{Actual\ Resiquimod\ Loading}{Theoretical\ Resiquimod\ Loading} x100\%.$ Table S1 contains information of MC made for in vitro and in vivo studies.

Microconfetti size characterization

Scaffold and MC morphology were evaluated by scanning electron microscopy (SEM, Hitachi S-4700 Cold Cathode Field Emission). Scaffolds were mounted onto aluminum stubs using carbon tape and microconfetti were suspended in water and dried onto stubs.

Samples were coated with palladium using a sputter coater and imaged at 2 kV. Images of MC obtained on the SEM at various magnification were analyzed by ImageJ for dimensions. Dimension measurements were compiled from two different batches of MC with three unique SEM images per batch. Representative images of measurements taken for each size can be seen in Figure S2.

Microconfetti injectability

The ability to deliver a full dose of MC through a 26 G needle was determined by quantifying the amount of polymer expelled from the needle and comparing to a pipetted control. Small, medium, and large MC were suspended in PBS at a similar concentration to the vaccine formulation and 0.2 mL volumes were either injected through the needle or pipetted into microcentrifuge tubes. Samples were degraded into dextran by acid hydrolysis and bicinchoninic acid assay was run to determine the percent intended dose of MC, defined as the signal from samples injected through the needle, normalized to the pipetted sample.

Detection of endotoxin

MC samples were suspended in endotoxin-free water at 1 mg/mL and incubated at 4˚C overnight. Samples were assessed for presence of detectable endotoxin using the Pierce LAL Chromogenic Endotoxin Quantitation Kit (Thermo Fisher, Scientific, Waltham, MA) in accordance with manufacturer instructions. All samples had undetectable levels of endotoxin (< 0.1 EU/mg).

Characterization of resiquimod release profile

MC were suspended in microcentrifuge tubes containing 1X phosphate buffered saline (PBS, pH 7.4) at 1 mg/mL and incubated at 37°C on a shaker plate at 150 RPM. At specific time points, samples were centrifuged for 20 minutes and the supernatant was separated from the pellet. Both samples were stored at −20°C until the end of the study. Resiquimod release was quantified by reading fluorescence of the supernatant diluted in DMSO on a plate reader (excitation: 260 nm, emission: 360 nm) and normalized to fully degraded by incubation at 80°C for several days.

Characterization of ovalbumin adsorption by flow cytometry

BODIPY-MC was incubated at 5 mg MC/mL in a solution of ovalbumin (OVA) conjugated to TexasRed dye (Thermo Fisher Scientific) at 50 μg/mL in PBS for 20 minutes at room temperature. Samples were washed three times with PBS to remove any un-adsorbed OVA and then ran on the flow cytometer (Attune NxT, Thermo Fisher Scientific) at a concentration of 0.1 mg/mL with respect to MC.

Isolation and culture of bone marrow derived dendritic cells

BMDCs were obtained from C57BL/6J mice or B6CBAF1/J mice (Jackson Laboratory, Bar Harbor, ME) and cultured 8–10 days prior to using in Dulbecco’s Modified Eagle Medium (DMEM, Corning, Corning, NY) supplemented with 1% penicillin-streptomycin (Hyclone, Pittsburgh, PA), 10% fetal bovine serum (Corning), and 10 ng/mL granulocyte-macrophage

colony-stimulating factor (GM-CSF, Thermo Fisher Scientific). Fresh media was added every other day until use.

Cell lines and cell culture

B3Z (CD8+) and KZO (CD4+) T cell hybridoma lines with β-galactosidase reporters for IL-2 were a kind gift from Dr. Nilabh Shastri (Johns Hopkins University). B3Z/KZO cells were cultured in RPMI 1640 media (VWR, Radnor, PA) supplemented with L-glutamine (2.05 mM), 1 mM sodium pyruvate (Gibco, Thermo Fisher Scientific), 1% penicillin-streptomycin, 10% fetal bovine serum, and 50 μM 2-mercaptoethanol. The immortalized dendritic cell line, DC2.4, was used for MHC I presentation assay (B3Z). DC2.4 cells were obtained from Sigma (St. Louis, MO) and cultured in RPMI 1640 supplemented with L-glutamine (2.05 mM), HEPES (25 mM), 1% nonessential amino acids (Gibco), 1% penicillin-streptomycin, 10% fetal bovine serum, and 50 μM 2-mercaptoethanol. BMDCs derived from B6CBAF1/J mice were used for the MHC II presentation assay (KZO). The immortalized macrophage cell line, RAW 264.7 (ATCC, Manassas, VA), was cultured in DMEM supplemented with 1% penicillin-streptomycin, 10% fetal bovine serum. All cells were cultured at 37˚C with 5% CO2 and 100% relative humidity.

Characterization of bone marrow derived dendritic cell cytotoxicity

BMDCs from C57BL/6J mice were plated in 96-well plates overnight at 50,000 cells per well in 0.1 mL of media containing 10 ng/mL GM-CSF. The next day, MC at a range of concentrations (500 – 15.6 μg/mL) in 0.1 mL was added to the cells and incubated for 24 hours. Blank and resiquimod-loaded MC (1% w/w) were evaluated. Cytotoxicity was measured by the Pierce LDH Cytotoxicity Assay Kit (Thermo Fisher Scientific) in accordance with manufacturer instructions. Percent cytotoxicity was reported by normalizing signal to the control of cells treated with lysis buffer (100% death). Supernatant was collected and stored at −20˚C for cytokine analysis.

Detection of cytokine secretion by ELISA

Cytokine secretion was measured in the supernatant of BMDCs treated with MC for 24 hours by enzyme-linked immunosorbent assay (ELISA). TNF-α, IL-1β, and IL-6 were measured in accordance with manufacturer instructions (eBioscience, Thermo Fisher Scientific).

Detection of MHC presentation of ovalbumin peptide

DC2.4 or BMDCs derived from B6CBAF1/J (Jackson Labs) were plated in 96-well plates at 50,000 cells per well in 0.1 mL overnight for MHC I and MHC II presentation, respectively. The next day, cells were treated with 10 μg/mL OVA (EndoFit, InvivoGen, San Diego, CA) and MC (500 – 15.6 μg/mL) suspended in media. 0.1 mL containing 100,000 p/KZO (MHC I/II) cells were introduced immediately after treating cells and co-incubated for 24 hours. Presentation was determined by β-galactosidase activity, indicative of IL-2 production. Cell culture media was replaced with 0.1 mL of solution containing 0.155 mM chlorophenol red β-D-galactopyranoside, 0.125% Nonidet P-40 Alternative, and 9 mM $MgCl_2$ in PBS. Plates

were sealed and incubated at room temperature for 14 hours and then 75 μL supernatant was transferred to a new plate and absorbance was read on a plate reader (570 nm).

Microconfetti internalization by confocal microscopy

Chambered coverglass slides (Thermo Fisher Scientific) with a surface area of 0.7 cm^2 per well were coated with poly-D-lysine in water (75 μg/mL) for at least 4 hours, and then washed 3x with water. BMDCs from C57BL/6J mice were seeded into chambers overnight at 200,000 cells/well. Cells were treated with 12.5 μg of BODIPY-MC for 24 hours. Cells were stained with CellTracker Blue CMAC dye (Thermo Fisher Scientific) and LysoTracker Deep Red dye (Thermo Fisher Scientific) in accordance with manufacturer instructions and were then live imaged on a confocal microscope (Zeiss LSM 710 Spectral Confocal Laser Scanning Microscope). Tile scans were taken at the center of the well and then z-stacks were obtained in the tiles along the diagonals of the tile scans to reduce sample bias. Uptake was confirmed by z-stacks, where MC were labeled as internalized when CellTracker Blue CMAC dye surrounded the entire circumference of the MC. The percent of cells with internalized MC was calculated by normalizing number of cells with one or more MC internalized to the total number of cells within a z-stack frame. Number of medium and large MC internalized per cell was also counted in z-stacks. Z-stacks were converted into maximum intensity projections and 3-rendererd images using the Imaris microscopy image analysis software (Oxford Instruments, Concord, MA). The same method was repeated with the cell lines, DC2.4 and RAW 264.7, which were seeded at 35,000 and 50,000 cells per well, respectively, to account for different cell growth rates.

Preparation of microconfetti vaccine and immunization of mice

C57BL/6J mice (6–8 weeks old) were obtained from Jackson Labs. Mice were immunized subcutaneously in the flank with 0.2 mL using a 26-gauge needle. All mice in groups with OVA received 10 μg OVA per dose. MC were suspended in sterile PBS at a concentration 2x of the final injection concentration and sonicated for 10 minutes. MC were then mixed 1:1 with 2x OVA solution (0.1 mg/mL) in PBS and incubated at room temperature for 20 minutes prior to injection. Alum vaccine was prepared by incubating Alhydrogel (InvivoGen, San Diego, CA) at 2.5 mg/mL with 2x OVA solution (0.1 mg/mL) for 20 minutes prior to injection. To test the effect of resiquimod dose on the humoral response, vaccine groups (n = 4 per group) included PBS, OVA, Alum, soluble resiquimod at various doses (0.02, 0.1, 1, or 10 μg), and resiquimod loaded MC to match the soluble resiquimod doses. MC resiquimod loading was targeted to maintain ~ 1 mg of MC per dose for each resiquimod dose. Depending on the encapsulation efficiency of resiquimod loading, the ultimate MC dose was then adjusted to maintain 0.02, 0.1, 1, or 10 μg resiquimod (Table S1). Mice were immunized on day 0 and received a boost on day 21. To evaluate the effect of MC size on the humoral and cellular immune responses, mice were immunized on day 0, and received a boost on days 21 and 35. Vaccine groups (n = 5 per group) included PBS, OVA, Alum, resiquimod-loaded MC (small, medium, and large), and blank MC (small, medium, and large). The dose of resiquimod-loaded MC was adjusted to maintain 10 μg resiquimod, depending on the resiquimod encapsulation efficiency. Blank MC were delivered at the same dose as their resiquimod-loaded MC counterpart (Table S1).

Quantification of ovalbumin antibody titers

Serum was collected on Days −7 (prior to initial Day 0 vaccination), 28, and 42. Blood was collected by a submandibular bleed and samples were centrifuged at 4,000 x g for 10 min at 4˚C to separate the serum from the clot. Serum was then collected and stored at −80˚C until further analysis. Anti-OVA IgG and IgG2c antibody titers were quantified by ELISA. High-affinity 96-well plates were coated with 5 μg/mL OVA and incubated overnight at 4˚C. Plates were then washed three times with wash buffer (0.05% Tween 20 in PBS), and then blocked with blocking buffer (5% non-fat milk in PBS) for two hours at room temperature. After three more rounds of washing, serum serially diluted in blocking buffer was added to plates and incubated overnight at 4˚C. Plates were washed three times and then incubated with HRP-conjugated anti-IgG or anti-IgG2c secondary antibodies (Southern Biotech, Birmingham, AL) for 1 hour at room temperature. Plates were washed five times to remove the secondary antibody and developed with the addition of 3,3′,5,5′-tetramethylbenzidine (TMB) solution for 15 or 30 minutes for IgG and IgG2c, respectively. After the addition of 1 M sulfuric acid to terminate development, absorbance was measured on a plate reader (450 nm). Trendlines were applied to antibody dilutions for each mouse and endpoint antibody titers were solved for as the dilution to reach an absorbance optical density (OD) of 1. Endpoint titers were reported log transformed.

Statistical analysis

Statistical analysis was performed using GraphPad Prism (La Jolla, CA). Group comparisons were made by ANOVA, followed by Tukey's multiple comparisons post-test, to determine statistical significance.

Supplementary Material

Refer to Web version on PubMed Central for supplementary material.

ACKNOWLEDGEMENT

This work was performed in part at the Chapel Hill Analytical and Nanofabrication Laboratory, CHANL, a member of the North Carolina Research Triangle Nanotechnology Network, RTNN, which is supported by the National Science Foundation, Grant ECCS-1542015, as part of the National Nanotechnology Coordinated Infrastructure, NNCI. We thank the Small Animal Imaging Facility at the UNC Biomedical Imaging Research Center for providing the IVIS imaging service, and the imaging core is supported in part by an NCI cancer core grant, P30-CA016086-40. The Microscopy Services Laboratory, Department of Pathology and Laboratory Medicine, is supported in part by P30 CA016086 Cancer Center Core Support Grant to the UNC Lineberger Comprehensive Cancer Center. The UNC Flow Cytometry Core Facility is supported in part by P30 CA016086 Cancer Center Core Support Grant to the UNC Lineberger Comprehensive Cancer Center. Research reported in this publication was supported in part by the North Carolina Biotech Center Institutional Support Grant 2017-IDG-1025 and by the National Institutes of Health 1UM2AI30836-01. The content is solely the responsibility of the authors and does not necessarily represent the official views of the National Institutes of Health.

Funding Sources

This work was supported by UNC internal funds and NSF-GRFP (DGE-1650116).

ABBREVIATIONS

APC	antigen presenting cell

PAMP	pathogen-associated molecular pattern
TLR	toll-like receptor
PLGA	poly lactic-co-glycolic acid
GM-CSF	granulocyte-macrophage colony-stimulating factor
MSR	mesoporous silica rod
MC	microconfetti
Ace-DEX	acetalated dextran
BMDC	bone marrow derived dendritic cell
OVA	ovalbumin
MFI	median fluorescence intensity
MHC	major histocompatibility complex
ICG	indocyanine green
TEA	triethylamine
DMSO	dimethylsulfoxide
SEM	scanning electron microscopy
PBS	phosphate buffered saline
DMEM	Dulbecco's Modified Eagle Medium
ELISA	enzyme-linked immunosorbent assay
TMB	3,3′,5,5′-tetramethylbenzidine

REFERENCES

(1). Calabro S; Tritto E; Pezzotti A; Taccone M; Muzzi A; Bertholet S; De Gregorio E; O'Hagan DT; Baudner B; Seubert A The Adjuvant Effect of Mf59 Is Due to the Oil-in-Water Emulsion Formulation, None of the Individual Components Induce a Comparable Adjuvant Effect. Vaccine 2013, 31 (33), 3363–9, DOI: 10.1016/j.vaccine.2013.05.007. [PubMed: 23684834]

(2). Shi S; Zhu H; Xia X; Liang Z; Ma X; Sun B Vaccine Adjuvants: Understanding the Structure and Mechanism of Adjuvanticity. Vaccine 2019, 37 (24), 3167–3178, DOI: 10.1016/j.vaccine.2019.04.055. [PubMed: 31047671]

(3). O'Hagan DT; Ott GS; De Gregorio E; Seubert A The Mechanism of Action of Mf59 - an Innately Attractive Adjuvant Formulation. Vaccine 2012, 30 (29), 4341–8, DOI: S0264–410X(11)01468-X [pii] 10.1016/j.vaccine.2011.09.061. [PubMed: 22682289]

(4). Morel S; Didierlaurent A; Bourguignon P; Delhaye S; Baras B; Jacob V; Planty C; Elouahabi A; Harvengt P; Carlsen H; Kielland A; Chomez P; Garcon N; Van Mechelen M Adjuvant System As03 Containing A-Tocopherol Modulates Innate Immune Response and Leads to Improved Adaptive Immunity. Vaccine 2011, 29 (13), 2461–73, DOI: 10.1016/j.vaccine.2011.01.011. [PubMed: 21256188]

(5). Kaisho T; Akira S Toll-Like Receptors as Adjuvant Receptors. Biochim Biophys Acta 2002, 1589 (1), 1–13, DOI: 10.1016/s0167-4889(01)00182-3. [PubMed: 11909637]

(6). McKee AS; Marrack P Old and New Adjuvants. Curr Opin Immunol 2017, 47, 44–51, DOI: 10.1016/j.coi.2017.06.005. [PubMed: 28734174]

(7). Tomai MA; Vasilakos JP Tlr-7 and −8 Agonists as Vaccine Adjuvants. Expert Rev Vaccines 2011, 10 (4), 405–7, DOI: 10.1586/erv.11.26. [PubMed: 21506636]

(8). TL W; CL A; AM C; SJ G; RL M; RM S; MJ R; JP V; MA T Modulation of Th1 and Th2 Cytokine Production with the Immune Response Modifiers, R-848 and Imiquimod. Cellular immunology 1999, 191 (1), DOI: 10.1006/cimm.1998.1406.

(9). Gallovic MD; Schully KL; Bell MG; Elberson MA; Palmer JR; Darko CA; Bachelder EM; Wyslouzil BE; Keane-Myers AM; Ainslie KM Acetalated Dextran Microparticulate Vaccine Formulated Via Coaxial Electrospray Preserves Toxin Neutralization and Enhances Murine Survival Following Inhalational Bacillus Anthracis Exposure. Adv Healthc Mater 2016, DOI: 10.1002/adhm.201600642.

(10). Schully KL; Sharma S; Peine KJ; Pesce J; Elberson MA; Fonseca ME; Prouty AM; Bell MG; Borteh H; Gallovic M; Bachelder EM; Keane-Myers A; Ainslie KM Rapid Vaccination Using an Acetalated Dextran Microparticulate Subunit Vaccine Confers Protection against Triplicate Challenge by Bacillus Anthracis. Pharm Res 2013, 30 (5), 1349–61, DOI: 10.1007/s11095-013-0975-x. [PubMed: 23354770]

(11). Schully KL; Bell MG; Prouty AM; Gallovic MD; Gautam S; Peine KJ; Sharma S; Bachelder EM; Pesce JT; Elberson MA; Ainslie KM; Keane-Myers A Evaluation of a Biodegradable Microparticulate Polymer as a Carrier for Burkholderia Pseudomallei Subunit Vaccines in a Mouse Model of Melioidosis. Int J Pharm 2015, 495 (2), 849–61, DOI: 10.1016/j.ijpharm.2015.09.059. [PubMed: 26428631]

(12). Sabado RL; Pavlick A; Gnjatic S; Cruz CM; Vengco I; Hasan F; Spadaccia M; Darvishian F; Chiriboga L; Holman RM; Escalon J; Muren C; Escano C; Yepes E; Sharpe D; Vasilakos JP; Rolnitzsky L; Goldberg JD; Mandeli J; Adams S; Jungbluth A; Pan L; Venhaus R; Ott PA; Bhardwaj N Resiquimod as an Immunologic Adjuvant for Ny-Eso-1 Protein Vaccination in Patients with High-Risk Melanoma. Cancer Immunol Res 2015, 3 (3), 278–87, DOI: 2326–6066.CIR-14–0202 [pii] 10.1158/2326-6066.CIR-14-0202. [PubMed: 25633712]

(13). Otero M; Calarota SA; Felber B; Laddy D; Pavlakis G; Boyer JD; Weiner DB Resiquimod Is a Modest Adjuvant for Hiv-1 Gag-Based Genetic Immunization in a Mouse Model. Vaccine 2004, 22 (13–14), 1782–90, DOI: 10.1016/j.vaccine.2004.01.037 S0264410X04001021 [pii]. [PubMed: 15068862]

(14). Didierlaurent AM; Morel S; Lockman L; Giannini SL; Bisteau M; Carlsen H; Kielland A; Vosters O; Vanderheyde N; Schiavetti F; Larocque D; Van Mechelen M; Garçon N As04, an Aluminum Salt- and Tlr4 Agonist-Based Adjuvant System, Induces a Transient Localized Innate Immune Response Leading to Enhanced Adaptive Immunity. The Journal of Immunology 2009, 183 (10), 6186, DOI: 10.4049/jimmunol.0901474. [PubMed: 19864596]

(15). Herrin DM; Coates EE; Costner PJ; Kemp TJ; Nason MC; Saharia KK; Pan Y; Sarwar UN; Holman L; Yamshchikov G; Koup RA; Pang YYS; Seder RA; Schiller JT; Graham BS; Pinto LA; Ledgerwood JE Comparison of Adaptive and Innate Immune Responses Induced by Licensed Vaccines for Human Papillomavirus. Hum Vaccin Immunother 2014, 10 (12), 3446–54, DOI: 10.4161/hv.34408. [PubMed: 25483691]

(16). Ali OA; Doherty E; Mooney DJ; Emerich D Relationship of Vaccine Efficacy to the Kinetics of Dc and T-Cell Responses Induced by Plg-Based Cancer Vaccines. Biomatter 2011, 1 (1), 66–75, DOI: 10.4161/biom.1.1.16277. [PubMed: 23507728]

(17). Singh A; Qin H; Fernandez I; Wei J; Lin J; Kwak LW; Roy K An Injectable Synthetic Immune-Priming Center Mediates Efficient T-Cell Class Switching and T-Helper 1 Response against B Cell Lymphoma. Journal of Controlled Release 2011, 155 (2), 184 – 192, DOI: 10.1016/j.jconrel.2011.06.008. [PubMed: 21708196]

(18). Shih TY; Blacklow SO; Li AW; Freedman BR; Bencherif S; Koshy ST; Darnell MC; Mooney DJ Injectable, Tough Alginate Cryogels as Cancer Vaccines. Adv Healthc Mater 2018, 7 (10), e1701469, DOI: 10.1002/adhm.201701469. [PubMed: 29441705]

(19). Song H; Huang P; Niu J; Shi G; Zhang C; Kong D; Wang W Injectable Polypeptide Hydrogel for Dual-Delivery of Antigen and Tlr3 Agonist to Modulate Dendritic Cells in Vivo and Enhance Potent Cytotoxic T-Lymphocyte Response against Melanoma. Biomaterials 2018, 159, 119–129, DOI: 10.1016/j.biomaterials.2018.01.004. [PubMed: 29324304]

(20). Liu Y; Xiao L; Joo KI; Hu B; Fang J; Wang P In Situ Modulation of Dendritic Cells by Injectable Thermosensitive Hydrogels for Cancer Vaccines in Mice. Biomacromolecules 2014, 15 (10), 3836–45, DOI: 10.1021/bm501166j. [PubMed: 25207465]

(21). Wu Y; Wei W; Zhou M; Wang Y; Wu J; Ma G; Su Z Thermal-Sensitive Hydrogel as Adjuvant-Free Vaccine Delivery System for H5n1 Intranasal Immunization. Biomaterials 2012, 33 (7), 2351–60, DOI: 10.1016/j.biomaterials.2011.11.068. [PubMed: 22192540]

(22). Wei J; Xue W; Yu X; Qiu X; Liu Z Ph Sensitive Phosphorylated Chitosan Hydrogel as Vaccine Delivery System for Intramuscular Immunization. J Biomater Appl 2017, 31 (10), 1358–1369, DOI: 10.1177/0885328217704139. [PubMed: 28387574]

(23). Chen R; Ma H; Zhang L; Bryers JD Precision-Porous Templated Scaffolds of Varying Pore Size Drive Dendritic Cell Activation. Biotechnol Bioeng 2018, 115 (4), 1086–1095, DOI: 10.1002/bit.26532. [PubMed: 29280498]

(24). Kim J; Li WA; Choi Y; Lewin SA; Verbeke CS; Dranoff G; Mooney DJ Injectable, Spontaneously Assembling, Inorganic Scaffolds Modulate Immune Cells in Vivo and Increase Vaccine Efficacy. Nat Biotechnol 2015, 33 (1), 64–72, DOI: 10.1038/nbt.3071. [PubMed: 25485616]

(25). Choi Y; Jeong JH; Kim J Mechanically Enhanced Hierarchically Porous Scaffold Composed of Mesoporous Silica for Host Immune Cell Recruitment. Adv Healthc Mater 2017, 6 (8), DOI: 10.1002/adhm.201601160.

(26). Li AW; Sobral MC; Badrinath S; Choi Y; Graveline A; Stafford AG; Weaver JC; Dellacherie MO; Shih TY; Ali OA; Kim J; Wucherpfennig KW; Mooney DJ A Facile Approach to Enhance Antigen Response for Personalized Cancer Vaccination. Nat Mater 2018, DOI: 10.1038/s41563-018-0028-2.

(27). Gause KT; Wheatley AK; Cui J; Yan Y; Kent SJ; Caruso F Immunological Principles Guiding the Rational Design of Particles for Vaccine Delivery. ACS Nano 2017, 11 (1), 54–68, DOI: 10.1021/acsnano.6b07343. [PubMed: 28075558]

(28). Chen N; Kroger CJ; Tisch RM; Bachelder EM; Ainslie KM Prevention of Type 1 Diabetes with Acetalated Dextran Microparticles Containing Rapamycin and Pancreatic Peptide P31. Adv Healthc Mater 2018, 7 (18), e1800341, DOI: 10.1002/adhm.201800341. [PubMed: 30051618]

(29). Collier MA; Gallovic MD; Bachelder EM; Sykes CD; Kashuba A; Ainslie KM Saquinavir Loaded Acetalated Dextran Microconfetti – a Long Acting Protease Inhibitor Injectable. Pharm Res 2016, 33 (8), 1998–2009, DOI: 10.1007/s11095-016-1936-y. [PubMed: 27154460]

(30). Graham-Gurysh E; Moore KM; Satterlee AB; Sheets KT; Lin FC; Bachelder EM; Miller CR; Hingtgen SD; Ainslie KM Sustained Delivery of Doxorubicin Via Acetalated Dextran Scaffold Prevents Glioblastoma Recurrence after Surgical Resection. Mol Pharm 2018, 15 (3), 1309–1318, DOI: 10.1021/acs.molpharmaceut.7b01114. [PubMed: 29342360]

(31). Graham-Gurysh EG; Moore KM; Schorzman AN; Lee T; Zamboni WC; Hingtgen SD; Bachelder EM; Ainslie KM Tumor Responsive and Tunable Polymeric Platform for Optimized Delivery of Paclitaxel to Treat Glioblastoma. ACS Appl Mater Interfaces 2020, DOI: 10.1021/acsami.0c04102.

(32). Bachelder EM; Pino EN; Ainslie KM Acetalated Dextran: A Tunable and Acid-Labile Biopolymer with Facile Synthesis and a Range of Applications. Chem Rev 2017, 117 (3), 1915–1926, DOI: 10.1021/acs.chemrev.6b00532. [PubMed: 28032507]

(33). Broaders KE; Cohen JA; Beaudette TT; Bachelder EM; Frechet JM Acetalated Dextran Is a Chemically and Biologically Tunable Material for Particulate Immunotherapy. Proc Natl Acad Sci U S A 2009, 106 (14), 5497–502, DOI: 0901592106 [pii] 10.1073/pnas.0901592106. [PubMed: 19321415]

(34). Chen N; Gallovic MD; Tiet P; Ting JP; Ainslie KM; Bachelder EM Investigation of Tunable Acetalated Dextran Microparticle Platform to Optimize M2e-Based Influenza Vaccine Efficacy. J Control Release 2018, 289, 114–124, DOI: 10.1016/j.jconrel.2018.09.020. [PubMed: 30261204]

(35). Duong AD; Sharma S; Peine KJ; Gupta G; Satoskar AR; Bachelder EM; Wyslouzil BE; Ainslie KM Electrospray Encapsulation of Toll-Like Receptor Agonist Resiquimod in Polymer Microparticles for the Treatment of Visceral Leishmaniasis. Mol Pharm 2013, 10 (3), 1045–55, DOI: 10.1021/mp3005098. [PubMed: 23320733]

(36). Kauffman KJ; Do C; Sharma S; Gallovic MD; Bachelder EM; Ainslie KM Synthesis and Characterization of Acetalated Dextran Polymer and Microparticles with Ethanol as a Degradation Product. ACS Appl Mater Interfaces 2012, 4 (8), 4149–55, DOI: 10.1021/am3008888. [PubMed: 22833690]

(37). Banchereau J; Steinman RM Dendritic Cells and the Control of Immunity. Nature 1998, 392 (6673), 245–52, DOI: 10.1038/32588. [PubMed: 9521319]

(38). Agarwal R; Singh V; Jurney P; Shi L; Sreenivasan SV; Roy K Mammalian Cells Preferentially Internalize Hydrogel Nanodiscs over Nanorods and Use Shape-Specific Uptake Mechanisms. Proceedings of the National Academy of Sciences 2013, 110 (43), 17247–17252, DOI: 10.1073/pnas.1305000110.

(39). Kumar S; Anselmo AC; Banerjee A; Zakrewsky M; Mitragotri S Shape and Size-Dependent Immune Response to Antigen-Carrying Nanoparticles. 2015.

(40). Beletskii A; Galloway A; Rele S; Stone M; Malinoski F Engineered Print(®) Nanoparticles for Controlled Delivery of Antigens and Immunostimulants. Hum Vaccin Immunother 2014, 10 (7), 1908–13, DOI: 10.4161/hv.28817. [PubMed: 25424798]

(41). Champion JA; Mitragotri S Shape Induced Inhibition of Phagocytosis of Polymer Particles. Pharm Res 2009, 26 (1), 244–9, DOI: 10.1007/s11095-008-9626-z. [PubMed: 18548338]

(42). Champion JA; Mitragotri S Role of Target Geometry in Phagocytosis. Proc Natl Acad Sci U S A 2006, 103 (13), 4930–4. [PubMed: 16549762]

(43). Garapaty A; Champion JA Tunable Particles Alter Macrophage Uptake Based on Combinatorial Effects of Physical Properties. Bioeng Transl Med 2017, 2 (1), 92–101, DOI: 10.1002/btm2.10047. [PubMed: 29313025]

(44). Walkey CD, O. JB, G. H, E. A, C. WCW Nanoparticle Size and Surface Chemistry Determine Serum Protein Adsorption and Macrophage Uptake. Journal of the American Chemical Society 2012, 134 (4), 2139–2147, DOI: 10.1021/ja2084338. [PubMed: 22191645]

(45). Bamberger D, H. D, K. M, B. M, W. PR Surface Modification of Polysaccharide-Based Nanoparticles with Peg and Dextran and the Effects on Immune Cell Binding and Stimulatory Characteristics. Molecular Pharmaceutics 2017, 14 (12), 4403–4416, DOI: 10.1021/acs.molpharmaceut.7b00507. [PubMed: 29063757]

(46). Chang TZ; Stadmiller SS; Staskevicius E; Champion JA Effects of Ovalbumin Protein Nanoparticle Vaccine Size and Coating on Dendritic Cell Processing. Biomater Sci 2017, 5 (2), 223–233, DOI: 10.1039/c6bm00500d. [PubMed: 27918020]

(47). Curtsinger JM; Schmidt CS; Mondino A; Lins DC; Kedl RM; Jenkins MK; Mescher MF Inflammatory Cytokines Provide a Third Signal for Activation of Naive Cd4+ and Cd8+ T Cells. The Journal of Immunology 1999, 162 (6), 3256–3262. [PubMed: 10092777]

(48). Janeway CA; Travers P; Walport M; Shlomchik MJ Immunobiology: The Immune System in Health and Disease, 5th ed.; Garland Science: New York, 2001.

(49). Cox MA; Harrington LE; Zajac AJ Cytokines and the Inception of Cd8 T Cell Responses. Trends Immunol 2011, 32 (4), 180–6, DOI: 10.1016/j.it.2011.01.004. [PubMed: 21371940]

(50). Shen H; Ackerman AL; Cody V; Giodini A; Hinson ER; Cresswell P; Edelson RL; Saltzman WM; Hanlon DJ Enhanced and Prolonged Cross-Presentation Following Endosomal Escape of Exogenous Antigens Encapsulated in Biodegradable Nanoparticles. Immunology 2006, 117 (1), 78–88, DOI: IMM2268 [pii] 10.1111/j.1365-2567.2005.02268.x. [PubMed: 16423043]

(51). Bachelder EM; Beaudette TT; Broaders KE; Dashe J; Fréchet JMJ Acetal-Derivatized Dextran: An Acid-Responsive Biodegradable Material for Therapeutic Applications. Journal of the American Chemical Society 2008, 130 (32), 10494–10495, DOI: 10.1021/ja803947s. [PubMed: 18630909]

(52). Johnson MM; Collier MA; Hoang KV; Pino EN; Graham-Gurysh EG; Gallovic MD; Zahid MSH; Chen N; Schlesinger L; Gunn JS; Bachelder EM; Ainslie KM In Vivo and Cellular Trafficking of Acetalated Dextran Microparticles for Delivery of a Host-Directed Therapy for

Salmonella Enterica Serovar Typhi Infection. Mol Pharm 2018, 15 (11), 5336–5348, DOI: 10.1021/acs.molpharmaceut.8b00802. [PubMed: 30296381]

(53). Zhu J; Yamane H; Paul WE Differentiation of Effector Cd4 T Cell Populations. Annual Review of Immunology 2010, 28 (1), 445–489, DOI: 10.1146/annurev-immunol-030409-101212.

(54). Hogenesch H Mechanism of Immunopotentiation and Safety of Aluminum Adjuvants. Front Immunol 2012, 3, 406, DOI: 10.3389/fimmu.2012.00406. [PubMed: 23335921]

(55). Brugnolo F; Sampognaro S; Liotta F; Cosmi L; Annunziato F; Manuelli C; Campi P; Maggi E; Romagnani S; Parronchi P The Novel Synthetic Immune Response Modifier R-848 (Resiquimod) Shifts Human Allergen-Specific Cd4+ Th2 Lymphocytes into Ifn-Γ–Producing Cells. Journal of Allergy and Clinical Immunology 2003, 111 (2), 380 – 388, DOI: 10.1067/mai.2003.102. [PubMed: 12589360]

(56). Wang Q; Tan MT; Keegan BP; Barry MA; Heffernan MJ Time Course Study of the Antigen-Specific Immune Response to a Plga Microparticle Vaccine Formulation. Biomaterials 2014, 35 (29), 8385–8393. [PubMed: 24986256]

(57). Kim J; Li WA; Sands W; Mooney DJ Effect of Pore Structure of Macroporous Poly(Lactide-Co-Glycolide) Scaffolds on the in Vivo Enrichment of Dendritic Cells. ACS Appl Mater Interfaces 2014, 6 (11), 8505–12, DOI: 10.1021/am501376n. [PubMed: 24844318]

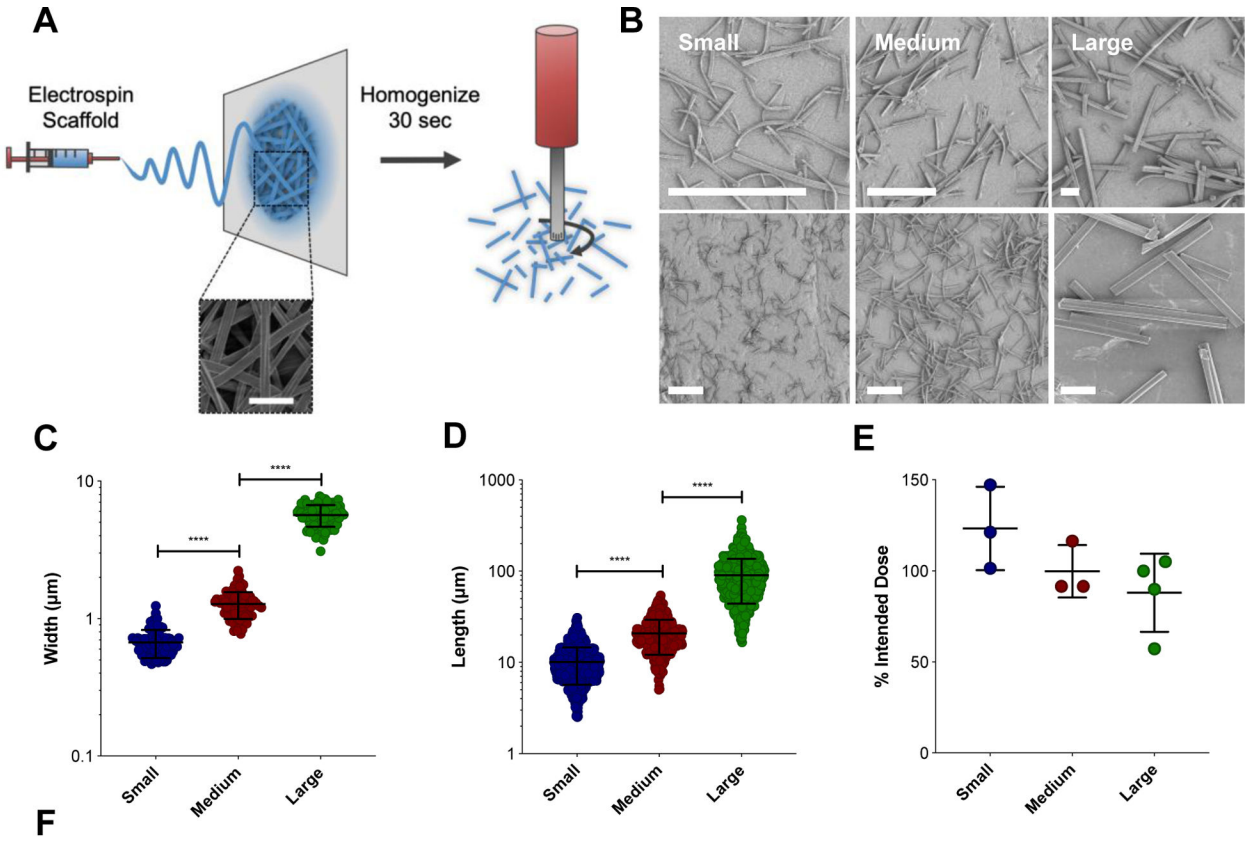

F

Microconfetti Size	Concentration (mg/mL)	Flow Rate (mL/hr)	Width (μm)	Length (μm)	Aspect Ratio	Resiquimod Loading (% w/w)	Encapsulation Efficiency (%)
Small	225	0.25	0.67 ± 0.16	10.2 ± 4.45	15.1	0.937 ± 0.018	93.7 ± 1.77
Medium	300	1.00	1.28 ± 0.28	20.7 ± 8.61	16.2	0.999 ± 0.046	99.9 ± 4.60
Large	400	4.00	5.67 ± 1.01	90.2 ± 46.3	15.9	1.12 ± 0.014	112 ± 1.40

Figure 1.

Fabrication of MC. (A) Schematic of MC fabrication. Ace-DEX scaffolds are electrospun and then homogenized to fragment the fibers into MC. Representative scanning electron micrograph of electrospun scaffold. Scale bar is 5 μm. (B) Scanning electron micrographs of small, medium, and large MC at different magnifications. Scale bar is 25 μm. Width (C) and length (D) measurements taken by ImageJ. Data represented as mean ± standard error of the mean. (E) Injectability of MC through a 26 G needle. Increments of 0.2 mL were pushed through the needle, degraded, and normalized to 0.2 mL of that volume pipetted to represent the intended MC dose. (F) Table containing electrospinning fabrication parameters (polymer concentration and flow rate) and resulting MC dimensions (length, width, and aspect ratio). Aspect ratio calculated by the average length divided by width. Data represented as mean ± standard deviation. MC: microconfetti. ****$p < 0.0001$.

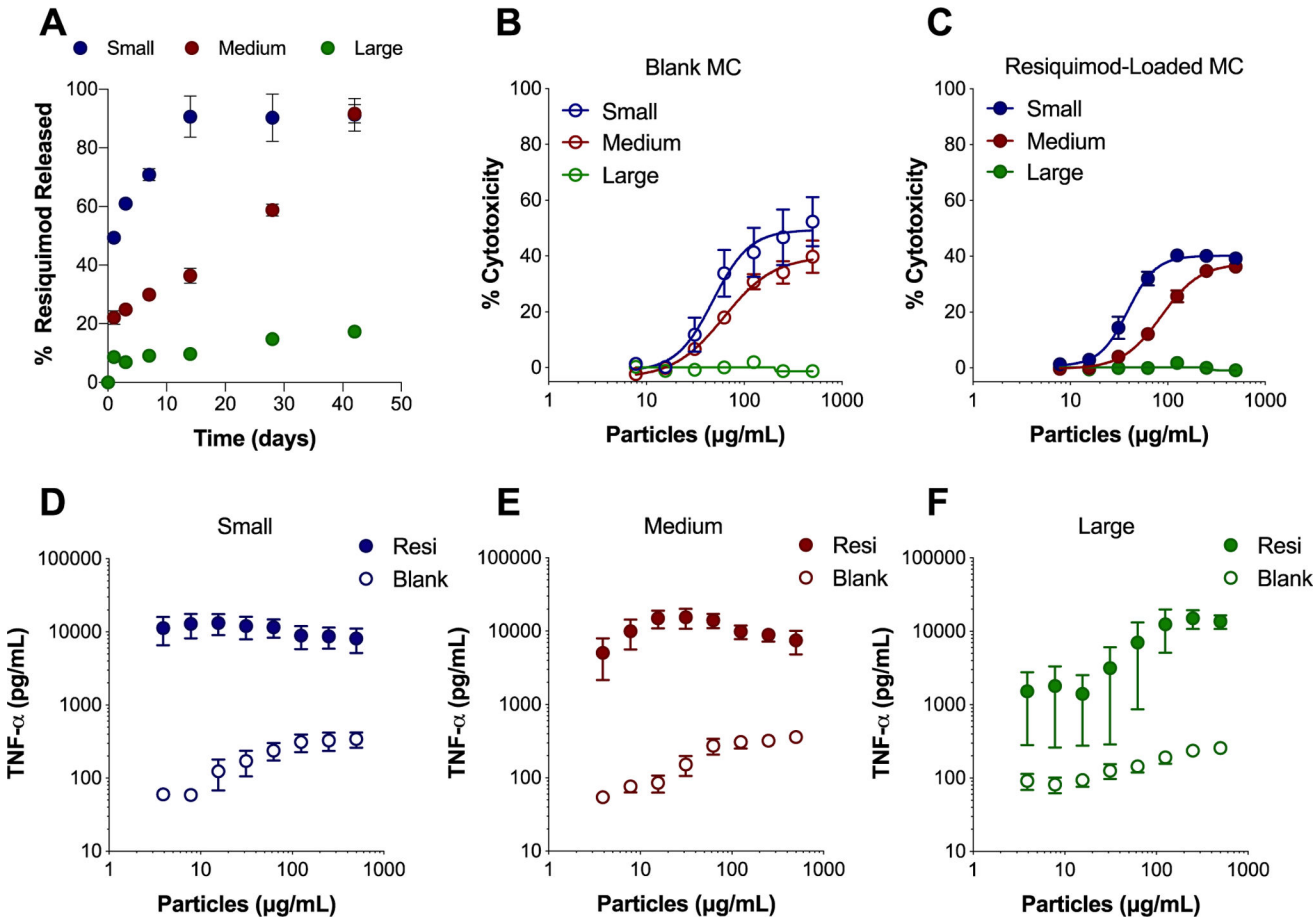

Figure 2.

In vitro MC resiquimod release profile and bioactivity in BMDCs. (A) Percent (%) of resiquimod released over time in PBS at pH 7.4 from small, medium, and large MC. Cytotoxicity of blank MC (B) and resiquimod-loaded MC (C) after incubation with BMDCs for 24 hours as determined by LDH assay. Supernatants from BMDCs treated for 24 hours with blank (open symbols) and resiquimod-loaded (closed symbols) small MC (D), medium MC (E), and large MC (F) were evaluated for TNF-α secretion by ELISA. Independent experiments (n = 2 – 4) in triplicate were performed. Data represented as mean ± standard error of the mean. BMDCs: bone marrow derived dendritic cells, MC: microconfetti, MPs: electrosprayed microparticles, resi: resiquimod.

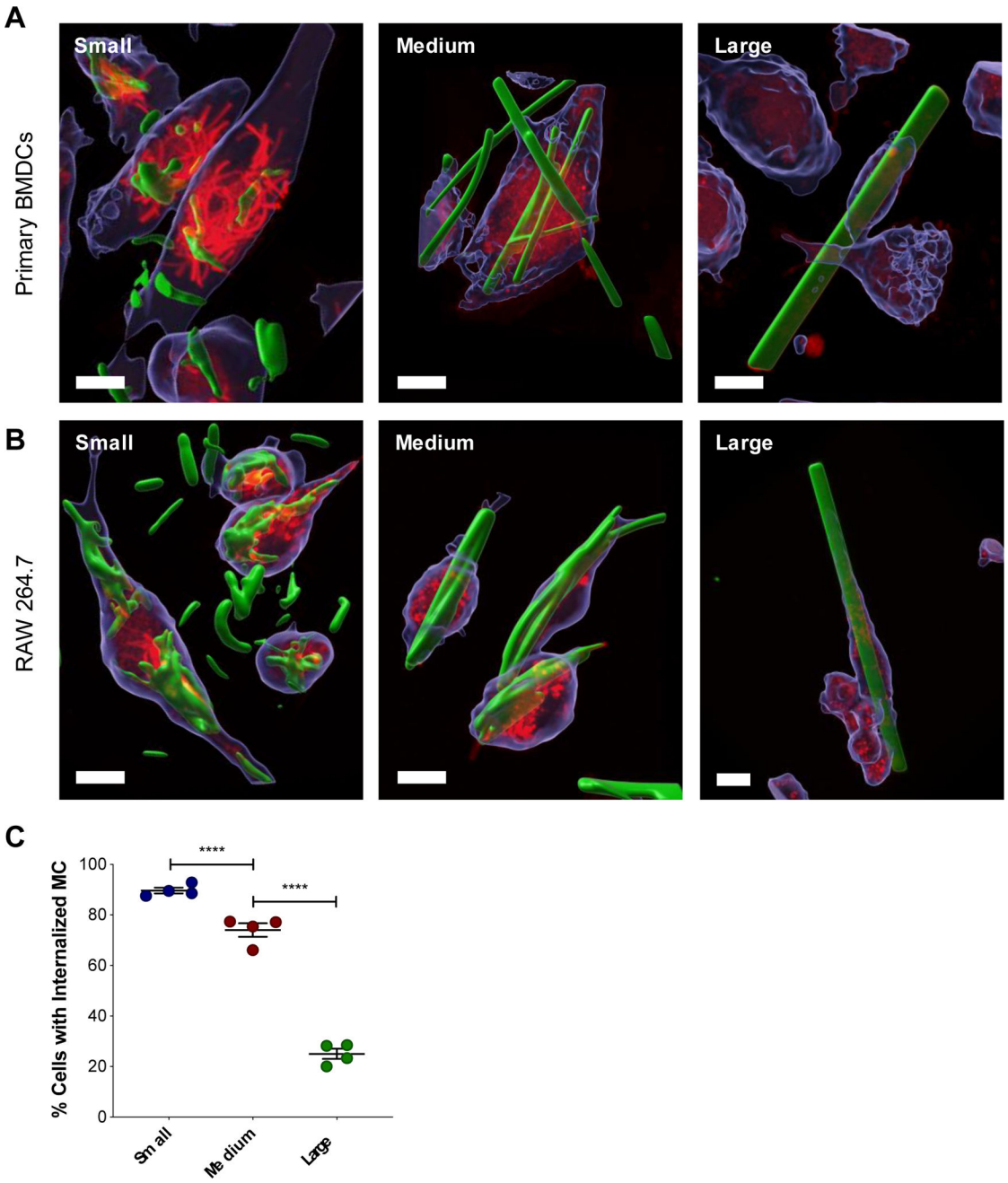

Figure 3.

(A) Confocal microscopy of MC internalization by APCs. Representative 3D renderings of z-stacks created in the Imaris microscopy image analysis software displaying MC internalized within BMDCs (A) and RAW 264.7 cells (B). Cells were treated with BODIPY-MC (green) for 24 hours and then stained with CellTracker (blue) and LysoTracker (red). Scale bar is 10 μm. (C) Quantification of MC internalization after 24 hours verified by z-stack. Percent of cells with one or more internalized MC. Data represented as mean ± standard error of the mean. **$p < 0.01$, ****$p < 0.0001$.

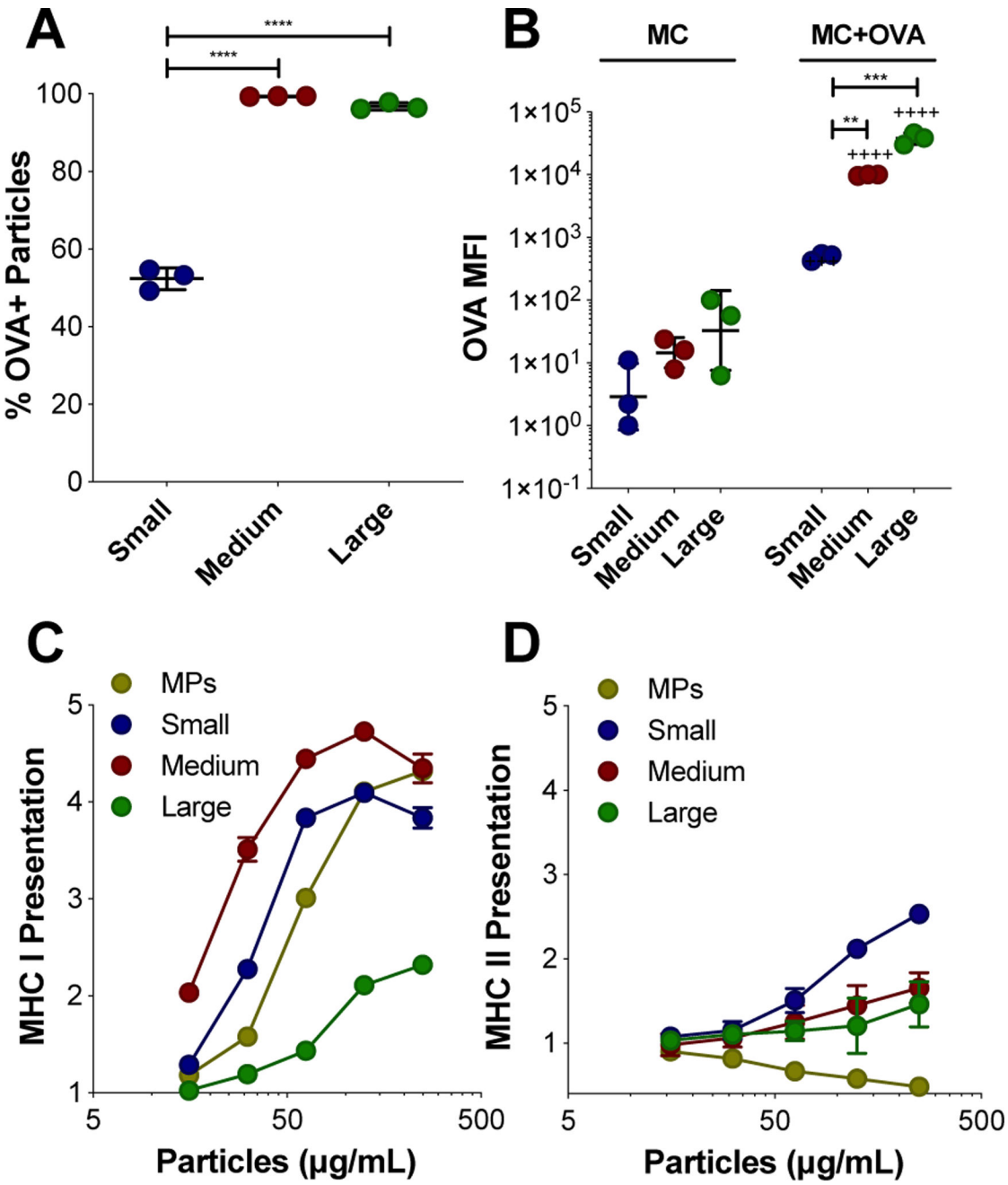

Figure 4.

OVA adsorption to MC surface and presentation of OVA. (A-B) Adsorption of Texas Red-OVA to the surface of small, medium, and large BODIPY-MC was characterized by flow cytometry. (A) Percent (%) of MC that are OVA+. (B) OVA adsorption represented by OVA median fluorescence intensity (MFI) for MC incubated without and with OVA. Relative MHC I (C) and II (D) presentation of OVA peptide facilitated by blank-MC after 24 hours, normalized to soluble OVA alone and compared to microparticles (MPs). Data represented as mean ± standard deviation. **p < 0.01, ***p < 0.0005, ****p < 0.0001 for comparisons

between MC sizes. +++$p < 0.0005$, ++++$p < 0.0001$ for comparisons between MC of the same size with and without OVA incubation.

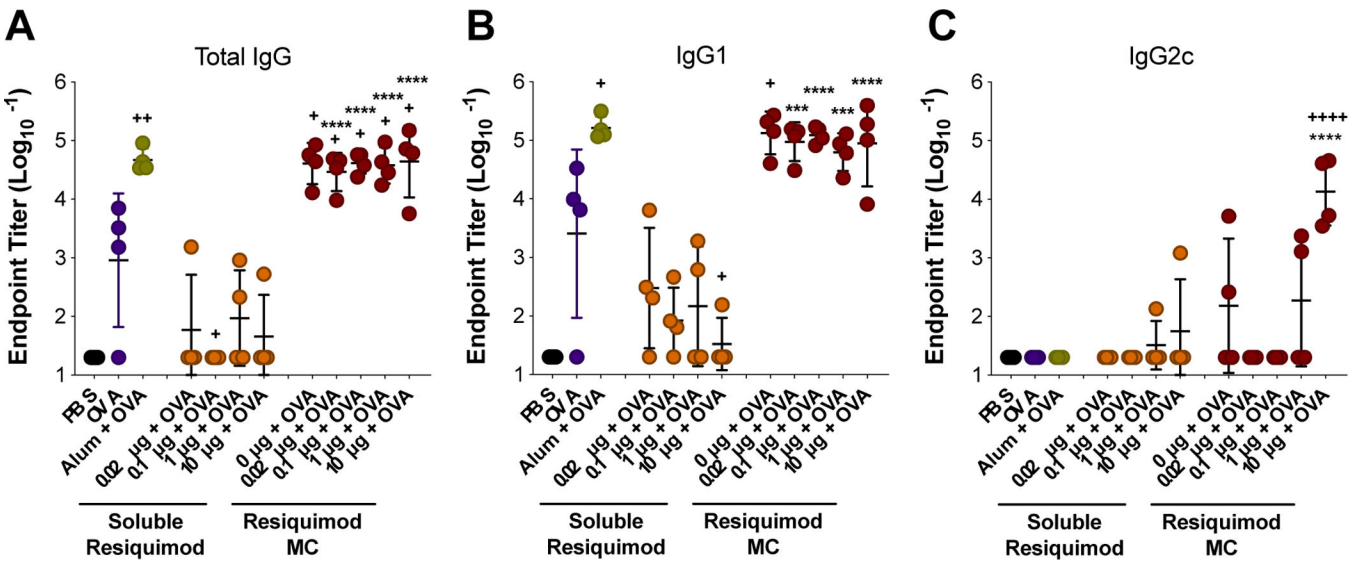

Figure 5.

Resiquimod dose vaccine study with medium sized MC. Mice were immunized on Day 0 (prime) and Day 21 (boost). Blood draws were done on Days −7 and 28. Total IgG (A), IgG1 (B), and IgG2c (C) endpoint anti-OVA antibody titers from day 28. Titers were log transformed and represented as mean ± standard deviation. ***p < 0.0005, ****p < 0.0001 for comparisons to soluble resiquimod dose counterpart. +p < 0.05, ++p < 0.01, ++++p < 0.0001 for comparisons to OVA only.

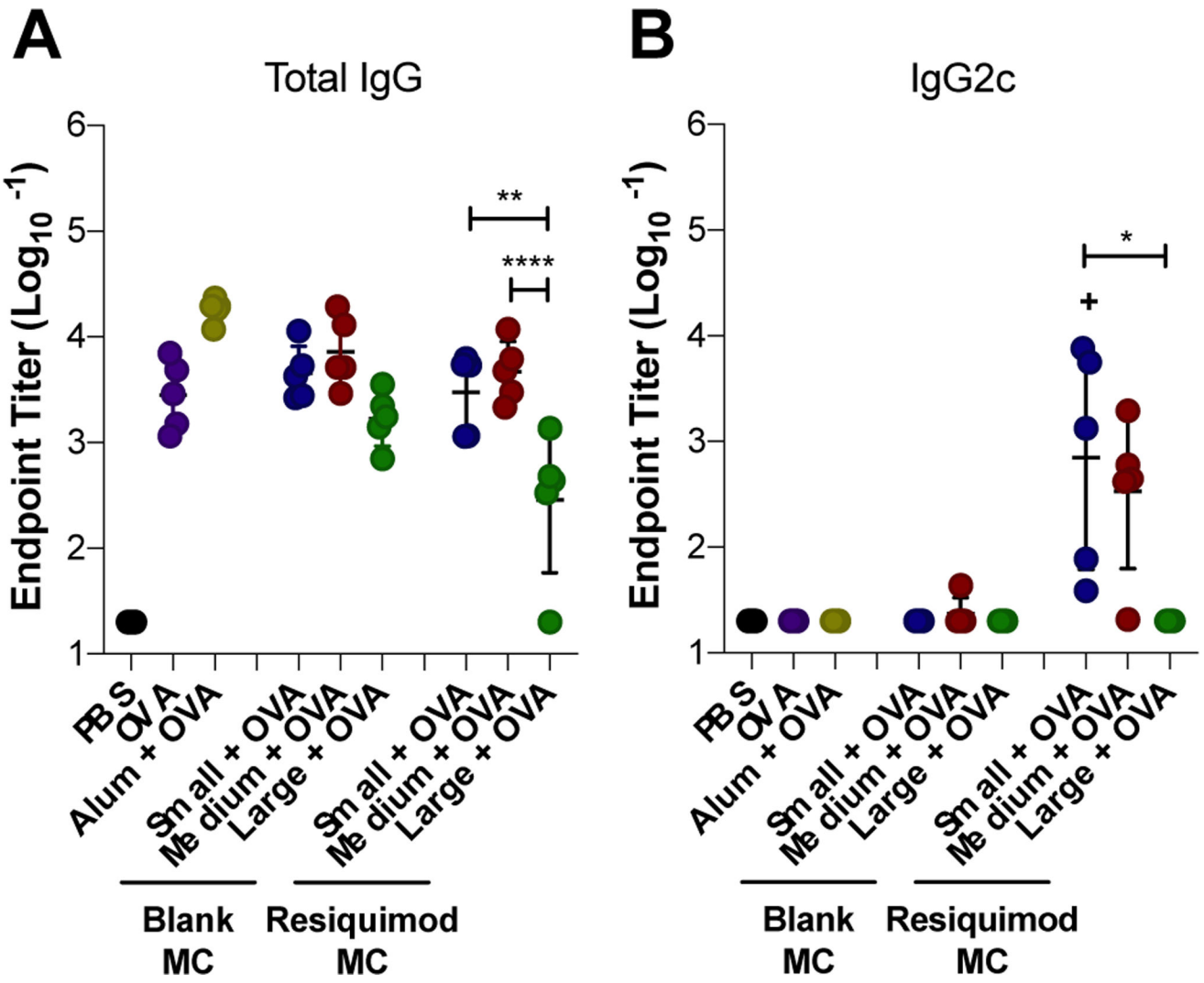

Figure 6.

Effect of MC size on the humoral immune response to ovalbumin vaccine. Mice were immunized on Day 0 (prime), Day 21 (boost), and Day 35 (boost). Total IgG (A), and IgG2c (B) endpoint anti-OVA antibody titers from Day 42 serum collection. Titers were log transformed and represented as mean ± standard deviation. *$p < 0.05$, **$p < 0.01$, ****$p < 0.0001$ for comparisons between MC sizes. +$p < 0.05$ for comparisons to OVA only.